



Subseasonal shift in tropical cyclone genesis over the western North Pacific in 2013

Yumi Choi¹ · Kyung-Ja Ha¹

Received: 6 March 2017 / Accepted: 21 September 2017 / Published online: 30 September 2017
© Springer-Verlag GmbH Germany 2017

Abstract The 2013 subseasonal asymmetry in tropical cyclone (TC) genesis over the western North Pacific (WNP) was investigated by using the 1979–2013 RSMC best track dataset. The genesis frequency of the 2013 WNP TCs between June–August (summer) and September–November (fall) manifested an abnormal temporal asymmetry: fewer typhoons (more tropical storms) in summer and more typhoons (normal tropical storms) in fall. The 2013 active summer-tropical storm genesis arose from both a failure of eastward extension of monsoon confluence region, especially in August and a lack of moisture supply for TC genesis over the eastern part of WNP, and consequently from fewer probability to reach typhoon intensity due to the westward movement of favorable location for genesis. Thereafter, the eastward extension of monsoon shear line in September and the establishment of monsoon gyre in October induced the eastward movement of favorable location for genesis which increased probability to reach typhoon intensity. The relative contribution of mid-level relative humidity to the positive GPI change played a major role in favorable condition for typhoon genesis in September (45.2%) and October (50.9%). The monsoon gyre pattern played a leading role in the most active fall-typhoon in 2013

This paper is a contribution to the special issue on East Asian Climate under Global Warming: Understanding and Projection, consisting of papers from the East Asian Climate (EAC) community and the 13th EAC International Workshop in Beijing, China on 24–25 March 2016, and coordinated by Jianping Li, Huang-Hsiung Hsu, Wei-Chyung Wang, Kyung-Ja Ha, Tim Li, and Akio Kitoh.

✉ Kyung-Ja Ha
kjha@pusan.ac.kr

¹ Division of Earth Environmental System, Pusan National University, Busan 609-735, Republic of Korea

contributing to the highest number of October-typhoon. The eastward-migration of convection mainly contributed to the subseasonal shift of TC genesis location following eastward movement of local SST warming from summer to fall under the La Niña-like neutral state. The enhanced active boreal summer intraseasonal oscillation (BSISO) in fall provided more favorable conditions for TC genesis showing about twice as many TCs occurred regarding BSISO in fall than those in summer. This spatiotemporal asymmetry in the large-scale circulations and moisture conditions between summer and fall accounted for the subseasonal shift of genesis location of TCs, and consequently for the active summer-tropical storm genesis and the active fall-typhoon genesis in 2013.

Keywords Genesis frequency · Genesis location · Subseasonal shift · Monsoon shear line · Monsoon confluence region · Monsoon gyre · Monsoon trough · BSISO · SST gradient

1 Introduction

The western North Pacific (WNP) is a warm pool that can provide abundant thermodynamic resources for tropical cyclone (TC) genesis throughout most of the year and thus the most active basin for TC genesis. It may result in the overestimated-role of underlying sea surface temperature (SST) in variability of both genesis frequency and intensity of TC relating to global warming (Webster et al. 2005). However, it has been demonstrated that changes in large-scale circulations play a more important role in modulating TC activity at least over the WNP (Chan 2008, 2009; Liu and Chan 2013; Park et al. 2013; Hsu et al. 2014; Choi et al. 2015; Lin and Chan 2015). The pioneering observational

study of Gray (1968, 1998) has shown that climatological genesis location of TCs meets the following necessary conditions composed of large-scale thermodynamic and dynamic parameters: warm water above at least 26.5 °C, high value of relative humidity in the mid-troposphere, high value of potential buoyancy in the low- to mid-troposphere, high value of relative vorticity in the low-troposphere, the minimum planetary vorticity in which region further away than about 5° latitude from the equator with a very few exceptions, and low value of vertical wind shear. This means that both thermodynamic and dynamic conditions should be adequate for TC genesis.

The WNP is a fertile basin for TC formation because monsoonal flows can supply abundant warm moist air and cyclonic vorticity in the lower level, thereby further organizing and enhancing moist convection. The canonical monsoon trough (MT) reveals the westerly monsoonal flows on its equatorward side and the easterlies on its poleward side (Gray 1968; Molinari and Vollaro 2013). The necessary thermodynamic and dynamic conditions for TC genesis are satisfied over the MT region (Harr and Wu 2011; Wu et al. 2012). Indeed, the approximately 85% of annual TCs (using the 1979–2013 climatological base period) occur from June to November, revealing the coincident variation with seasonal migration of MT. In addition, easterly waves can be accumulated over monsoon confluence region, which is the eastern edge of MT, and thus support TC genesis (Ritchie and Holland 1999; Roundy and Frank 2004). Therefore, location of the eastern edge of MT plays a crucial role in determining genesis location of TCs. Meanwhile, Zong and Wu (2015) defined MT axis as the line of zero-zonal wind with 850-hPa positive relative vorticity using the 850 hPa low-pass filtered winds after removal of the TC circulation. They determined that 43.1% of the total TCs occur within the MT region in May–October during the period of 2000–2010. In addition, they showed that most of the TCs occur in monsoon shear region because it has stronger low-level relative vorticity than the confluence zone. The results are inconsistent with those in Ritchie and Holland (1999) and Molinari and Vollaro (2013) due to the different definition and composite method of MT as well as the exclusion of monsoon gyre-related TC genesis.

The WNP TC genesis has been modulated by teleconnections on the various time scales through the changes in large-scale background states, which can be different in sub-regions over the WNP. The number of WNP TCs has decreased over the recent decades, experiencing significant decadal change over the southeastern part of WNP (Liu and Chan 2013; Hsu et al. 2014; Choi et al. 2015) especially in autumn (Hsu et al. 2014, 2017). On the interannual time scale, El Niño–Southern Oscillation (ENSO) is the most well-known modulator for TC genesis. In strong

El Niño-developing years, the number of TCs increases (decreases) over the southeastern (northwestern) part of the WNP in summer and fall because of the El Niño-induced equatorial lower-level westerlies (Wang and Chan 2002; Wang and Zhang 2002). After the developing years, TC formation is suppressed until the following spring and early summer over the entire WNP through the persisted lower-tropospheric anticyclone over the Philippine Sea (Wang et al. 2000; Wang and Chan 2002). In addition, the tropical Indian Ocean warming forces to emanate a warm atmospheric Kelvin wave into the Pacific, and the resultant surface divergence in the subtropics suppresses convection and induces anticyclonic anomalies over the subtropical Northwest Pacific in the boreal summer following strong El Niño years (Xie et al. 2009; Du et al. 2011), thereby decreasing the number of TC genesis (Du et al. 2011; Zhan et al. 2011). Furthermore, Yu et al. (2016) demonstrated that the tropical North Atlantic (TNA) SST anomaly (SSTA) is negatively correlated with the number of WNP TCs in July–October, changing low-level circulations over the tropical Indian Ocean through the air–sea interaction, and consequently modulating MT over the WNP.

The various spatiotemporal influences of the teleconnections may cause the different variations in the genesis frequency between weak- and intense-TCs, as invoked in previous studies (Frank and Young 2007; Zhan et al. 2011; Hsu et al. 2014). Zhan et al. (2011) demonstrated that the El Niño-forcing can change large-scale circulations over the southeastern part of the WNP, which is a favorable region for intense-TC genesis, whereas the tropical East Indian Ocean (EIO) SSTA can affect weak-TC genesis over the entire WNP. Frank and Yong (2007) discussed that the variability of the number of TCs depends on both the time and region to build up enough vorticity over the MT region that is thermodynamically adequate to promote convective instability.

From this point of view, the 2013 WNP TC genesis was very impressive showing a different temporal asymmetry in the genesis frequency between weak- and intense-TCS: inactive intense-TC and active weak-TC in summer (June–August) versus active intense-TC and normal weak-TC in fall (September–November) (Fig. 1). Ying et al. (2014) reported a review of the 2013 WNP TC activity associated with remote SST forcing from the equatorial eastern Pacific, seasonal migration of the East Asia summer monsoon, and intraseasonal oscillation (ISO) activity of 500-hPa geopotential height. We, however, focus on the subseasonal variance in the 2013 TC genesis between summer and fall, investigating changes in both large-scale environment conditions and ISOs activity. The WNP TC genesis is also significantly modulated by ISOs (Maloney and Hartmann 2001; Camargo et al. 2009; Mao and Wu 2010; Huang et al.

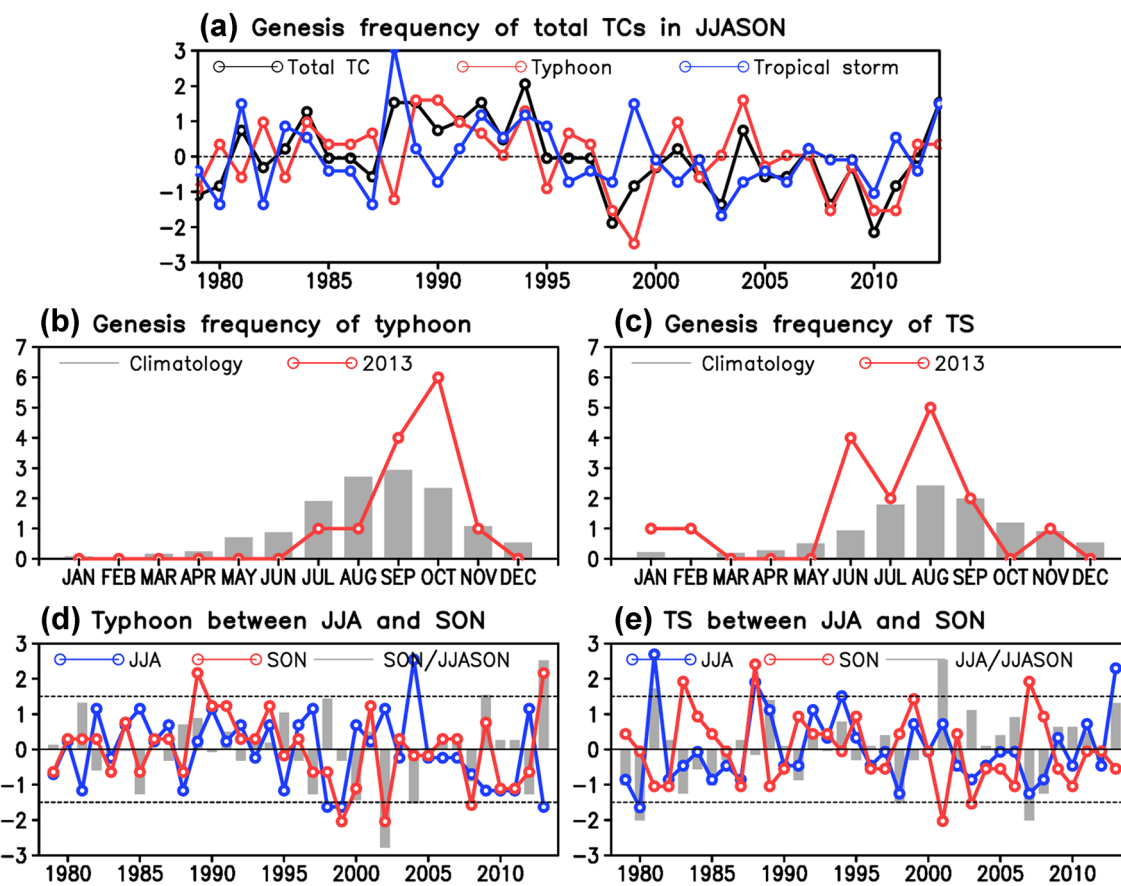


Fig. 1 Time series of the number of TCs over the western North Pacific (0° – 30° N, 100° – 180° E) for the period of 1979–2013. **a** Normalized genesis frequency of total TCs (more than 17.2 ms^{-1} , black solid line), typhoon (more than 32.6 ms^{-1} , red solid line), and tropical storm (17.2 – 32.5 ms^{-1} , blue solid line) in June–November. Monthly genesis frequency of **(b)** typhoon and **(c)** tropical storm in 2013 (red solid line) and those of the climatology (gray bar) using the base period of 1979–2013. Normalized subseasonal genesis frequency of

(d) typhoon and **(e)** tropical storm between June–August (blue solid line) and September–November (red solid line). **d, e** Gray bar denotes the number of typhoon (tropical storm) in September–November (June–August) divided by that of June–November. Black dotted lines denote 1.5 standard deviations. The best track dataset was obtained from the Regional Specialized Meteorological Center (RSMC) Tokyo-Typhoon Center

2011; Cao et al. 2012; Li and Zhou 2013; Kim and Seo 2016) through barotropic eddy kinetic energy conversion from lower-level mean flow (Maloney and Hartmann 2001; Mao and Wu 2010; Cao et al. 2012; Hsu et al. 2017) or control of midlevel relative humidity (Camargo et al. 2009). In this paper, the ISO activity was explored using two major boreal summer intraseasonal oscillations (BSISOs): a northward/northeastward propagating BSISO1 mode with periods of 30–60 days and a northward/northwestward propagating BSISO2 mode with periods of 10–30 days (Lee et al. 2013).

The next section describes details of data and method. Climatological seasonal variations in both large-scale environments and TC genesis and those of the 2013 subseasonal shift are presented in Sect. 3. Possible causes for the shift are addressed in Sect. 4. The last contains summary and discussion.

2 Data and analysis methods

2.1 Data

The best track dataset was obtained from the Regional Specialized Meteorological Center (RSMC) Tokyo-Typhoon Center for the period of 1979–2013, which is high quality era owing to operationally used satellite data. We classified TCs into two categories: typhoon (more than 32.6 ms^{-1}) and tropical storm (17.2 – 32.5 ms^{-1}) according to Saffir–Simpson scale (Song et al. 2010). Genesis is defined as the first record of a track over the WNP region (0° – 30° N, 100° – 180° E) in the RSMC best track dataset. The typhoon season is defined as June–November in which about 87% of annual typhoons occur over the WNP using base period of 1979–2013.

To investigate environmental conditions for the period 1979–2013, we used the daily ERA-Interim reanalysis

data produced by the European Centre for Medium-Range Weather Forecasts (ECMWF) (Dee et al. 2011) for atmospheric variables and obtained outgoing longwave radiation (OLR) from the National Oceanic and Atmospheric Administration (NOAA) (Liebmann and Smith 1996) which represents deep convection. The daily optimal interpolation SST (OISST) data (Reynolds et al. 2007) was used for the period 1982–2013. To isolate the synoptic-scale disturbances, but remain long-term mean (climatological background), we applied 7-day running mean to the datasets throughout the analysis (Huang et al. 2011). We obtained the monthly SST from the Hadley Centre Global Sea Ice and Sea Surface Temperature (HadISST) (Rayner et al. 2003).

2.2 GPI and moist thermodynamic condition

A modified genesis potential index (GPI) by Murakami and Wang (2010) was adopted to determine the influences of large-scale environment on TC genesis. The modified GPI improves an underestimate of large-scale condition for TC genesis over the region revealing strong upward motion such as the Intertropical Convergence Zone (ITCZ) by incorporating the vertical motion into the original GPI defined by Emanuel and Nolan (2004) (Murakami and Wang 2010). The modified version of GPI (hereafter referred to as GPI) is defined as

$$\left|10^5 \eta\right|^{\frac{3}{2}} \left(\frac{RH}{50}\right)^3 \left(\frac{V_{pot}}{70}\right)^3 (1 + 0.1V_s)^{-2} \left(\frac{-\omega + 0.1}{0.1}\right),$$

where η is the 850-hPa absolute vorticity (s^{-1}), RH is the 700-hPa relative humidity (%), V_{pot} is the potential intensity (PI) (ms^{-1}), V_s is the magnitude of the vertical wind shear (ms^{-1}) between the 200- and 850-hPa horizontal wind, and ω is the 500-hPa vertical wind velocity ($Pa s^{-1}$).

To quantitatively evaluate the relative contribution of each term to the GPI change, we used the modified method, first developed by Camargo et al. (2007), in Li et al. (2013) as follows.

$$\delta GPI = \alpha 1 \delta Term 1 + \alpha 2 \delta Term 2 + \alpha 3 \delta Term 3 + \alpha 4 \delta Term 4 + \alpha 5 \delta Term 5,$$

where coefficients are defined as

$$\alpha 1 = \overline{Term 2 \cdot Term 3 \cdot Term 4 \cdot Term 5}$$

$$\alpha 2 = \overline{Term 1 \cdot Term 3 \cdot Term 4 \cdot Term 5}$$

$$\alpha 3 = \overline{Term 1 \cdot Term 2 \cdot Term 4 \cdot Term 5}$$

$$\alpha 4 = \overline{Term 1 \cdot Term 2 \cdot Term 3 \cdot Term 5}$$

$$\alpha 5 = \overline{Term 1 \cdot Term 2 \cdot Term 3 \cdot Term 4}.$$

A bar and δ represent climatology and anomaly, respectively.

We adopted vertically integrated from 1000- to 100-hPa moisture flux convergence (MFC) which can be used to estimate precipitation associated with synoptic-scale systems (Oh and Ha 2015) and used the 850-hPa moisture transport to investigate large-scale moisture condition. MFC is defined as

$$MFC = -\nabla \cdot (qV_h),$$

where $q(kg kg^{-1})$ is the specific humidity and $V_h(ms^{-1})$ is the horizontal vector wind.

To describe thermodynamic state of an air parcel, we further used vertically averaged from 1000- to 500-hPa moisture static energy (MSE) composed of its enthalpy, potential energy, and latent energy. MSE is defined as

$$MSE = C_p T + gz + Lq,$$

where $C_p(1004 J kg^{-1} K^{-1})$ is the specific heat at constant pressure, $T(K)$ is the absolute air temperature, $g(9.81 ms^{-2})$ is the gravitational acceleration, $z(m)$ is the height, $L(2.5 \times 10^6 J kg^{-1})$ is the latent heat of evaporation, and $q(kg kg^{-1})$ is the specific humidity.

2.3 BSISO indices

To investigate influence of ISO on subseasonal shift in the WNP TC genesis, we adopted the BSISO indices proposed in Lee et al. (2013) which can capture both the canonical northward/northeastward propagating variability with periods of 30–60 days (BSISO1) and the northward/northwestward propagating variability with periods of 10–30 days (BSISO2) over the Asian summer monsoon region, involving no time filtering and thus being useful for monitoring and forecasting (see Figs. 2, 3 in Lee et al. 2013).

To define the BSISO indices, we applied multivariate empirical orthogonal function (MV-EOF) analysis to the daily OLR and 850-hPa zonal wind anomalies normalized by the area averaged temporal standard deviation over the Asian summer monsoon region ($10^{\circ}S$ – $40^{\circ}N$, 40° – $160^{\circ}E$) for the period of May–October. The anomalies were calculated by subtracting both the slow annual cycle (mean and first three harmonics of climatological annual variation using the 1981–2010 climatological base period) and the running mean of the last 120 days (the effect of interannual variability) from the original datasets. The first and second (third and fourth) MV-EOF modes are identified as the BSISO1 (BSISO2) modes. The projection coefficients (PCs) for the period of 1979–2013 were obtained by projecting OLR and U850 anomalies onto the EOF structures. Finally, the PCs of the leading four modes were used to define the BSISO1–1

(PC1), BSISO1-2 (PC2), BSISO2-1 (PC3), and BSISO2-2 (PC4), respectively.

Amplitude of BSISOs are defined as

$$\text{Amplitude}_{\text{BSISO1(BSISO2)}} = (\text{BSISO}_{\text{PC1(PC3)}}^2 + \text{BSISO}_{\text{PC2(PC4)}}^2)^{1/2}.$$

Active (inactive) BSISO is defined based on the amplitude more than (less than) 1.5.

3 Subseasonal shift in 2013

3.1 Climatological genesis frequency and location of the WNP TCs

Prior to investigating the 2013 TC genesis, climatological distributions of the WNP TC genesis should be understood. Figure 2 displays that monthly spatial distributions of genesis location of typhoon (red dot) and tropical storm (blue dot) during the period of 1979–2013 with climatological GPI and 850-hPa streamline. A distinct difference between two can be found that typhoon occurs further southeastward

or eastward and has a longer lifetime rather than those of tropical storm (Table 1). This result is consistent with the fact that genesis location of TCs is an informative indicator of potential intensity (Wang and Chan 2002; Ha et al. 2012; Choi et al. 2015) because TC intensity can be determined based on which largescale environments they have experienced throughout their lifetime. For instance, TCs occurred over the southeastern part of WNP have more opportunity to experience warm ocean, thereby easily reaching typhoon intensity.

The monthly climatological GPI fairly represents genesis location of TCs because GPI was developed based on climatological large-scale environments relating to TC genesis (Camargo et al. 2007, 2009; Murakami and Wang 2010). Monthly genesis location of TCs follows seasonal migration of monsoonal region as the large-scale patterns evolve with season (Fig. 2). Ritchie and Holland (1999) and Yoshida and Ishikawa (2013) identified that the distinct five large-scale patterns contributed to TC genesis: monsoon shear line, monsoon confluence region, monsoon gyre, easterly waves, and pre-existing TC. Monsoon shear line pattern is defined

Fig. 2 Spatial distributions of climatological genesis potential index (gray shading) and 850-hPa wind (streamline) in (a–f) June–November using the 1979–2013 climatological base period. The number of total TCs (more than 17.2 ms^{-1}), typhoon (more than 32.6 ms^{-1}), and tropical storm (17.2 – 32.5 ms^{-1}) is written at the top of each monthly panel. The genesis locations of typhoon and tropical storm are marked with red and blue dots, respectively

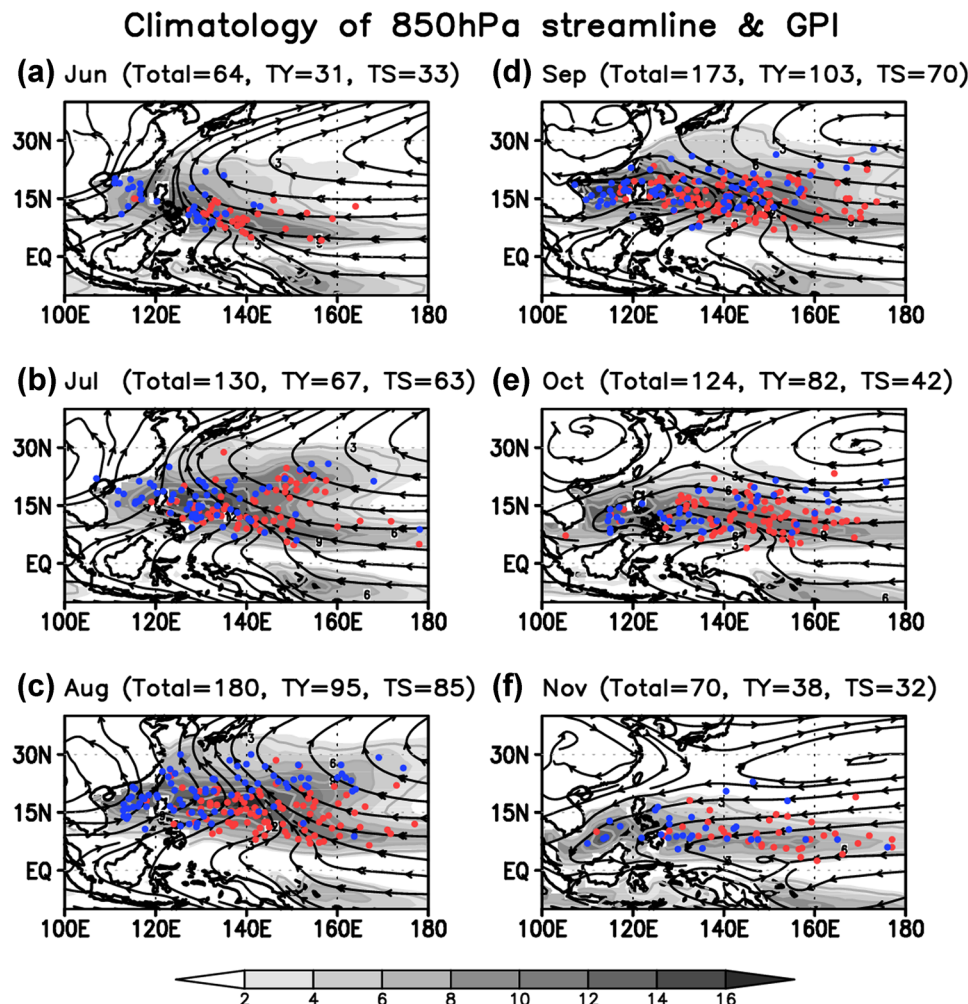


Table 1 Monthly climatology of genesis location and lifetime of TCs over the western North Pacific (0° – 30° N, 100° E– 180° E) in the typhoon season June–November using the 1979–2013 climatological base period: typhoon (typhoon categories 1–5; more than 32.6 ms^{-1}) and tropical storm (17.2 – 32.5 ms^{-1})

Month	Typhoon			Tropical storm		
	Longitude ($^{\circ}$ E)	Latitude ($^{\circ}$ N)	Lifetime (h)	Longitude ($^{\circ}$ E)	Latitude ($^{\circ}$ N)	Lifetime (h)
June	139.17	10.18	275.61	125.21	14.13	159.27
July	142.92	14.77	271.34	132.54	16.57	153.52
August	145.06	15.09	302.02	134.04	20.03	165.74
September	142.88	15.32	258.99	133.94	17.21	155.06
October	146.16	12.28	265.17	137.48	13.51	143.14
November	149.77	9.31	251.21	135.17	10.72	132.75

as a region of low sea level pressure (SLP) having westerly flow on the equatorward side throughout the 3 days before genesis. Monsoon confluence region is characterized by having westerly (easterly) flow on the west (east) side of genesis location and located in the east of the monsoon shear line or gyre. It is distinguished from the monsoon shear line by both having weaker westerlies on the equatorward side and higher SLP and interacting easterly waves. Easterly waves are defined a westward cyclonic perturbation embedded in the tropical easterlies below an upper-level anticyclonic circulation (Chen et al. 2008) within ITCZ which has confluent easterlies on equatorward and poleward sides (Ritchie and Holland 1999).

The monsoonal region extends northeastward showing migration of the monsoon confluence region toward east from June to August, as cross-equatorial flow develops and monsoonal westerlies extend eastward (Fig. 2a–c). In September, the mean flow regime along the 20° N changes into easterlies and the monsoon shear line and the monsoon confluence region become parallel to the latitude circle (Fig. 2d). This is consistent with the result that two major contribution flow patterns are the monsoon shear line and the monsoon confluence region accounted for above half of the total genesis events (Ritchie and Holland 1999; Yoshida and Ishikawa 2013). Since then, the MT retreats equatorward and become gyre structure (Huang et al. 2011) (Fig. 2e). In November, favorable location for genesis is confined along the equatorward of 15° N and occupied by the easterlies regime (Fig. 2f). A few TCs occurred beyond the monsoonal region might be influenced by the mid-latitude upper-tropospheric trough penetrations (Molinari and Vollaro 2012); or it might appear a lack of physical understanding of TC genesis regarding upper-level forcing or easterly waves (Chen et al. 2008).

3.2 Spatiotemporal asymmetry in the 2013 TC genesis

The 2013 WNP TC genesis in June–November ranked the highest number of total TCs (27), which was mostly attributed to active tropical storm, since 1995 during the analysis period of 1979–2013 (Fig. 1a). Regarding typhoon, the genesis frequency (13) was slightly above climatology

(11.89) showing normal genesis during the typhoon season. Meanwhile, subseasonal variation in the genesis frequency of TCs between summer and fall revealed a temporal asymmetry in typhoon and tropical storm: fewer typhoons (more tropical storms) in summer and more typhoons (normal tropical storms) in fall (Fig. 1b–e). The most active fall-typhoon in 2013 was attributed to the highest number of typhoon in October (6) during the analysis period (Fig. 1b, d). The number of typhoon remarkably increased from mid-September until early November with maxima in October (Table 2). In October, it is remarkable for almost the same genesis location of typhoon Wipha (149.0° E, 14.0° N) and intense-typhoon (above typhoon category 3 according to Saffir–Simpson scale; more than 48.9 ms^{-1}) Francisco (148.9° E, 13.8° N) (Table 2). In November, intense-typhoon Haiyan, ranked the strongest typhoon made landfall in recorded history, was generated at a latitude of 5.8° N close to the equator and moved westward staying over warm ocean throughout most of its lifetime (Fig. 3f). But conversely, only two typhoons occurred in summer which is suppressed compared with the climatology (5.5), whereas the number of tropical storm increased to 11 which is enhanced compared with the climatology (5.2) (Figs. 1, 3).

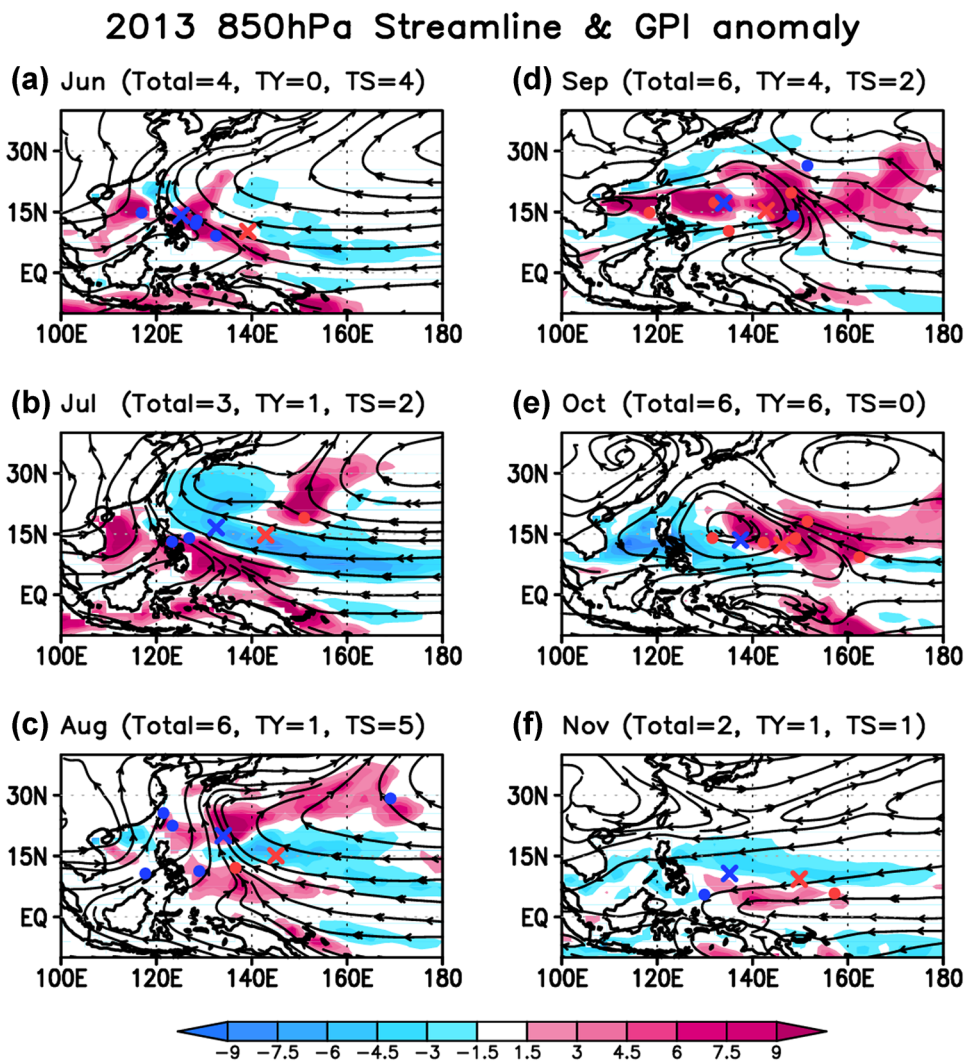
The 2013 temporal asymmetry in the genesis frequency of typhoon and tropical storm between summer and fall implies the fact that favorable location for genesis experienced a remarkable subseasonal shift from the west in summer to the east in fall. The positive GPI anomalies are fairly coincident with genesis location of TCs without a few cases, successfully revealing the subseasonal shift (Fig. 3). This result supports the fact that GPI can capture changes in the large-scale environment, which is responsible for the genesis frequency of TCs, on the intraseasonal time scale, but with a little lesser degree (Camargo et al. 2009). Compared with the climatology, the 2013 summer monsoon confluence region failed to extend eastward and was confined to the western part of the WNP, especially even in August, maintained near the 130° E (Fig. 3a–c). Thereafter, the monsoon shear line remarkably extended northeastward and the eastern edge of the MT located near the 150° E in September which means that the probability of typhoon genesis increases (Fig. 3d). Even though the

Table 2 A list of typhoon occurred over the western North Pacific (0° – 30° N, 100° E– 180° E) in 2013

Month	Date (ddhh)	Name	MSW (ms^{-1})	Longitude ($^{\circ}$ E)	Latitude ($^{\circ}$ N)
June	—	—	—	—	—
July	0700	Soulik	51.4	151.0	19.0
August	0812	Utor	53.97	136.6	12.1
September	1118	Man-Yi	33.41	148.1	19.7
	1600	Usagi	56.54	132.0	17.3
	2518	Wutip	33.41	118.4	14.8
	2906	Fitow	38.55	135.0	10.3
October	0100	Danas	46.3	151.5	18.1
	0812	Nari	38.55	131.6	14.0
	0900	Wipha	46.26	149.0	14.0
	1512	Francisco	53.97	148.9	13.8
	1900	Lekima	59.11	162.4	9.3
	2718	Krosa	38.55	142.3	12.9
November	0306	Haiyan	64.25	157.2	5.8

Typhoon is categorized according to the criteria of maximum sustained wind (MSW) more than 32.6 ms^{-1} . Names in bold indicate intense-typhoon (typhoon categories 3–5 according to Saffir–Simpson scale; more than 48.9 ms^{-1}). Genesis is defined as the first record of a track in the RSMC best track dataset

Fig. 3 Spatial distributions of 2013 monthly 850-hPa wind (streamline) and anomalous genesis potential index in (a–f) June–November. The number of total TCs (more than 17.2 ms^{-1}), typhoon (more than 32.6 ms^{-1}), and tropical storm (17.2 – 32.5 ms^{-1}) is written at the top of each monthly panel. The genesis locations of 2013 typhoon and tropical storm are marked with red and blue dots, respectively. The locations marked with an X are those climatology using the 1979–2013 climatological base period



MT failed to extend eastward in August, the TC genesis frequency in August (6) was the same to that in September (6). To demonstrate relative role of environmental factors in the genesis condition for TCs, we calculated quantitative contribution of each GPI term to the positive GPI change (Li et al. 2013) (Fig. 4). In August low-level absolute vorticity showed a negative contribution (-5.2%) to the GPI over the positive GPI change, whereas PI showed a positive contribution (40.1%) to the GPI over the region (Fig. 4c) revealing high MSE over the subtropical region (not shown). Molinari and Vollaro (2013) discussed the percentage of TC genesis over the long-term monthly mean MT, which is defined as positive 850-hPa relative vorticity, exceeds 80% in every month except July and August. In mid-summer, TCs tend to occur in the subtropics outside the MT than in any other month (see Figs. 1, 2 in Molinari and Vollaro 2013). It implies that contribution of MT activity to TC genesis frequency could be different between mid-summer and fall.

The 2013 October-typhoon genesis reveals an intriguing feature of the highest number of typhoon since 1979 associated with monsoon gyre pattern (Fig. 3e). Monsoon gyres are identified as a large diameter of cyclonic circulation over 2500 km (850-hPa maximum tangential wind between 800 and 1100 km radii), long-lasting above 4 days, and asymmetric precipitation peaked south and east of the gyre center (Lander 1994; Wu et al. 2013; Molinari and Vollaro 2017). Wu et al. (2013) demonstrated that approximately 20% of total TCs occur within or in the vicinity of monsoon gyres which generally form on the poleward side of the MT and frequently occur in August–October. Thus, the monsoon gyre pattern played a leading role in

the most active fall-typhoon in 2013 contributing to the highest number of typhoon in October (6). In addition, genesis of intense-typhoon Lekima (162.4°E, 9.3°N) might be influenced by the pre-existing intense-typhoon Francisco (148.9°E, 13.8°N), occurred 84 h prior to on the northeast of its genesis (Table 1) because pre-existing TCs influence new TC genesis on their southeast through the Rossby wave energy dispersion toward the southeast (Li and Fu 2006).

4 Possible causes

4.1 Eastward migration of convection region and local SST distribution

Monsoonal westerlies are a key component of the MT activity supplying abundant warm moist air and cyclonic vorticity to enhance moist convection, thereby developing and maintaining the MT by itself. Figure 5a displays time evolution of anomalous zonal wind averaged along the region 5° – 15° N from June to November in 2013. The zonal wind abruptly changed from easterlies to westerlies in mid-September and maintained until early November which is coincident with the sequence of the active fall-typhoon genesis (Table 2) relating to both the eastward extension of monsoon shear line in September and the establishment of monsoon gyre in October (Fig. 3d, e). Westerlies over the main formation region are favorable for TC genesis via both barotropic energy conversion from low-level mean flow (Maloney and Hartmann 2001; Mao and Wu 2010; Cao et al. 2012) and sustained moist convection (Ritchie and Holland 1999). The abrupt change in zonal wind was strongly coincident

Fig. 4 Relative contribution (%) of each term to the positive genesis potential index (GPI) change in (a–f) June–November. *Avor* absolute vorticity at 850 hPa, *RH700* relative humidity at 700 hPa, *PI* potential intensity, *VWS* vertical wind shear, *Ome500* omega at 500 hPa

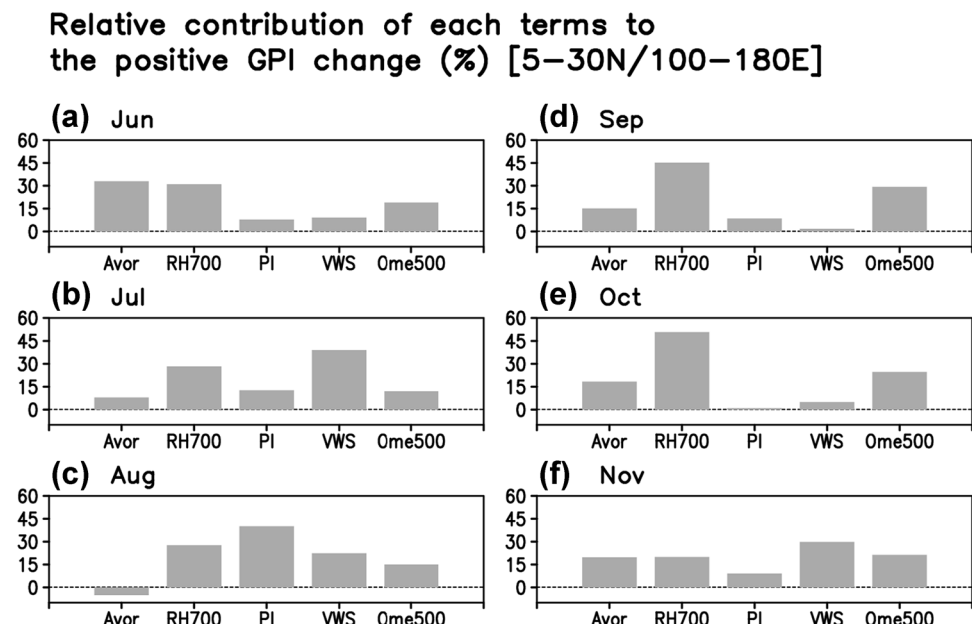
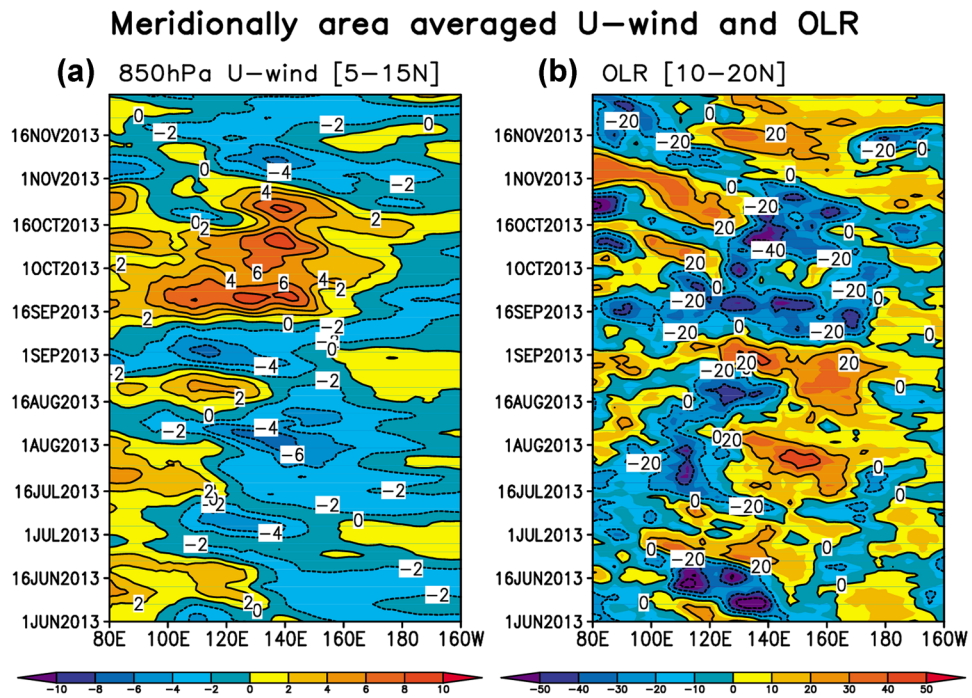


Fig. 5 Time evolution of 2013 daily anomalies of (a) 850-hPa zonal wind (ms^{-1}) and (b) OLR (Wm^{-2}) from June to November. Zonal wind and OLR are meridionally averaged over the regions (5° – 15° N) and (10° – 20° N), respectively



with the convection activity over the main formation region (10° – 20° N) revealing the eastward shift of the convection region from summer to fall (Fig. 5b).

To determine whether the teleconnections from eastern Pacific, Indian Ocean, and North Atlantic influenced the abrupt change in zonal wind and eastward migration of convection region, we analyzed time series of Nino 3.4, EIO, TNA indices (Fig. 6). La Niña-like neutral state and very weak EIO warming were displayed throughout most of the 2013 typhoon season. Even though the TNA warming, which is negatively correlated with the WNP genesis frequency (Yu et al. 2016), increased from June to October,

the genesis frequency did not decrease. Figure 7a shows that the eastward SST gradient could play a key role in the eastward-migration of convection revealing eastward movement of local SST warming from summer to fall. The eastward increase in convective instability (MSE) from June to October revealed the favorable thermodynamic state and high probability of typhoon genesis over the eastern part of WNP, and consequently increased the genesis frequency of typhoon in fall (Fig. 7b). It implies that the subseasonal shift in the 2013 WNP TC genesis arose from the change in local SST distribution, not the teleconnections.

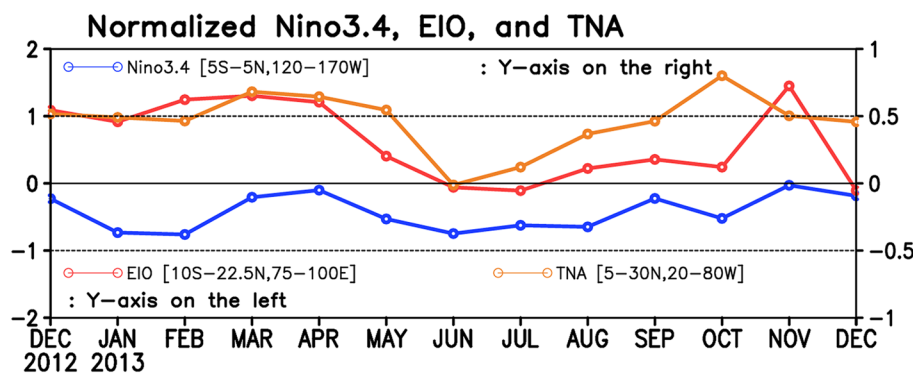


Fig. 6 The normalized time series of monthly Nino 3.4 index (blue solid line, y-axis on the right), which is SSTA averaged over the region (5° S– 5° N, 120° – 170° W), East Indian Ocean (EIO) index (red solid line, y-axis on the left), which is SSTA averaged over the region (10° S– 22.5° N, 75° – 100° E), and tropical North Atlantic (TNA) index

(orange solid line, y-axis on the right), which is SSTA averaged over the region (5° – 30° N, 20° – 80° W). Black dotted lines denote 1 and 0.5 standard deviations for EIO and TNA indices with y-axis on the left and Nino 3.4 index with y-axis on the right, respectively

Fig. 7 Time evolution of 2013 daily anomalies of (a, c) SST (shading, °C) and (b) moist static energy (shading, kJ kg^{-1}) vertically averaged from 1000–hPa to 500–hPa from June to November. Those are zonally and meridionally averaged over the regions (a, b) (5° – 20° N) and (c) (100° – 180° E), respectively. (a, c) The contours denote the climatology of SST obtained by using the 1982–2013 climatological base period

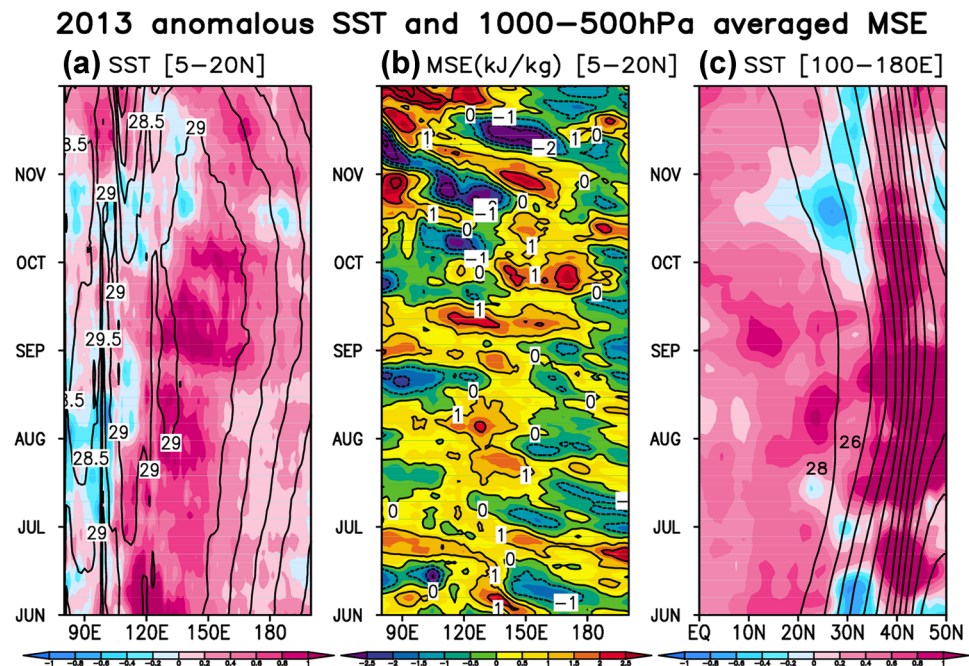
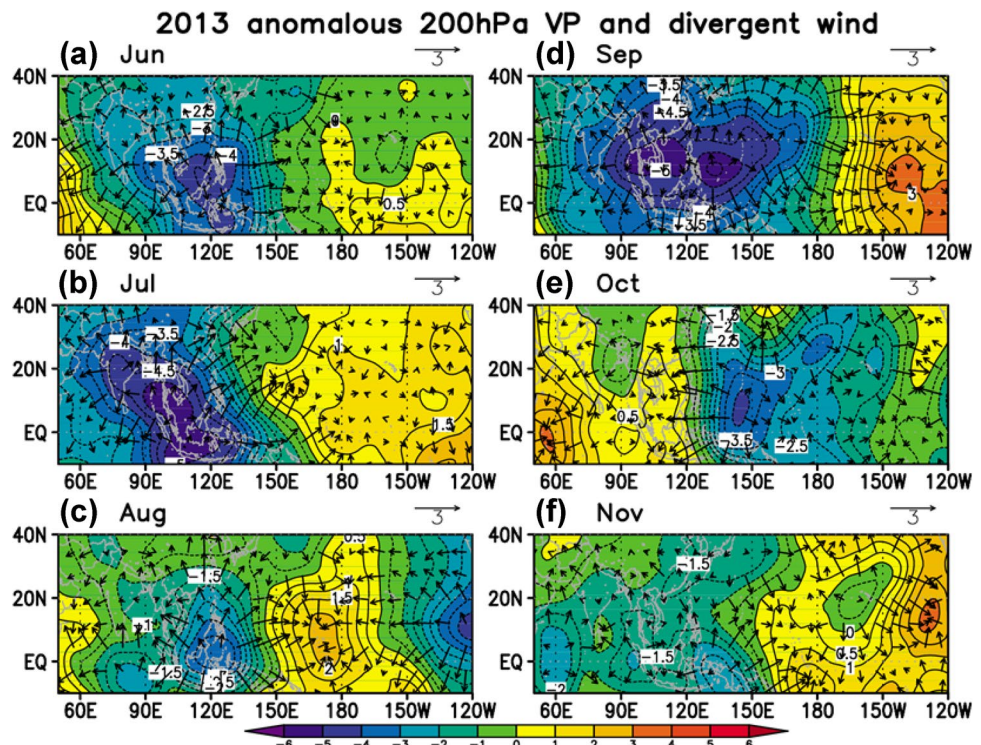


Figure 8 displays the spatial distributions of anomalous and 200-hPa velocity potential and divergent wind which are useful for distinguishing between the deep convection and the suppression. The center of enhanced convection region was located over the South China Sea in summer (Fig. 8a–c). In August, strong suppression over the eastern part of WNP near the date line further induced a local Walker circulation.

Fig. 8 Spatial distributions of 2013 monthly 200-hPa velocity potential (shading, 10^{-6} s^{-1}) and divergent wind (vector, ms^{-1}) anomalies in (a–f) June–November

The enhanced convection region confined to the western part of WNP resulted in the westward movement of genesis location of TCs compared with the climatology. The summer-TCs had fewer probability to reach typhoon intensity due to the relatively shorter life time, thus increasing the genesis frequency of tropical storm (Fig. 3a–c). In September, the enhanced deep convection over the main formation region



was strongly linked to the eastward extension of monsoon shear line (Fig. 8d), thereby increasing probability of typhoon genesis (Fig. 3d). Thereafter, the enhanced (suppressed) convection was located in the eastern (western) part of WNP, further inducing a local Walker circulation (Fig. 8e). Thus, the eastward movement of genesis location of TCs induced more probability of typhoon genesis due to the relatively longer life time in October. In addition, intense TCs tend to occur over the eastern part of the monsoon gyre (see Fig. 3 in Molinari and Vollaro 2017). The monsoon gyre in October also gave rise to the favorable condition for TC genesis east of the center, thereby increasing the genesis frequency of typhoon (Fig. 3e).

To investigate large-scale moisture condition, Fig. 9 displays the 850-hPa moisture transport and vertically integrated MFC anomalies from 1000- to 100-hPa which can be used to estimate precipitation associated with synoptic-scale systems (Oh and Ha 2015). In summer, the negative MFC anomalies were dominant over the eastern part of WNP (Fig. 9a–c) revealing a lack of moisture supply for TC genesis. Meanwhile, abundant moisture was provided by enhanced westerly over the main formation region with asymmetric precipitation peaked south and east of the monsoon shear line in September and east of the monsoon gyre in October (Fig. 9d, e). The westerlies over the main

formation region might be further intensified by the response to the diabatic heating over the east of the monsoon gyre (Gill 1980). This temporal asymmetry in the large-scale moisture condition between summer and fall also leads to the subseasonal shift of genesis location of TCs, and consequently to the active summer-tropical storm genesis and the active fall-typhoon genesis in 2013. Indeed, we found that relative contribution of mid-level relative humidity to the positive GPI change played a major role in favorable condition for typhoon genesis in September (45.2%) and October (50.9%) (Fig. 4d, e) which is consistent the result that the relative humidity is the most important factor contributing to TC genesis frequency on the intraseasonal time scale (Camaro et al. 2009).

The most active 2013 fall-typhoon attributed to the highest number of typhoon in October (6) which is strongly linked to the monsoon gyre. It is noted that remarkable zonal and meridional SST gradient occurred over the WNP in October (Fig. 7a, c). The northeastward extended monsoon shear line over the warm pool in September could be superposed with lower-level cyclonic vorticity via the Gill-type response to the warm SSTA (Gill 1980) over the southeastern part of WNP and consequently evolved into the monsoon gyre in October (Figs. 3, 7). In addition, the northward increase in SSTA along the 20–45°N in October decreased meridional thermal gradient, especially in the second half of October, and thus inducing the meandering subtropical jet via thermal wind balance (Fig. 10). The meandering jet induced upper-level divergence further enhanced upward motion around the 140°E (Fig. 10c). Indeed, the relative contribution of mid-level upward motion to the positive GPI change played a secondary role in favorable condition for typhoon genesis in October (24.7%) (Fig. 4e).

4.2 BSISO activity

Unlike the boreal winter ISO, which is an eastward propagating canonical Madden–Julian oscillation (MJO) along the equator, northward or northeastward propagating ISO is prominent in off-equatorial monsoon region in the boreal summer (Yun et al. 2008; Lee et al. 2013). In addition, there is a northward or northwestward propagating quasi-biweekly oscillation (QBWO) originated near the date line, which can also affect lower-level convection over the WNP (Lee et al. 2013; Li and Zhou 2013). Thus, we investigated influence of BSISO activity on the subseasonal shift in TC genesis using the BSISO indices proposed in Lee et al. (2013). BSISO1 mode is characterized as the northeastward propagating variability with periods of 30–60 days, whereas BSISO2 mode is characterized as the northward/northwestward propagating variability with periods of 10–30 days (see Figs. 9, 10 in Lee et al. 2013).

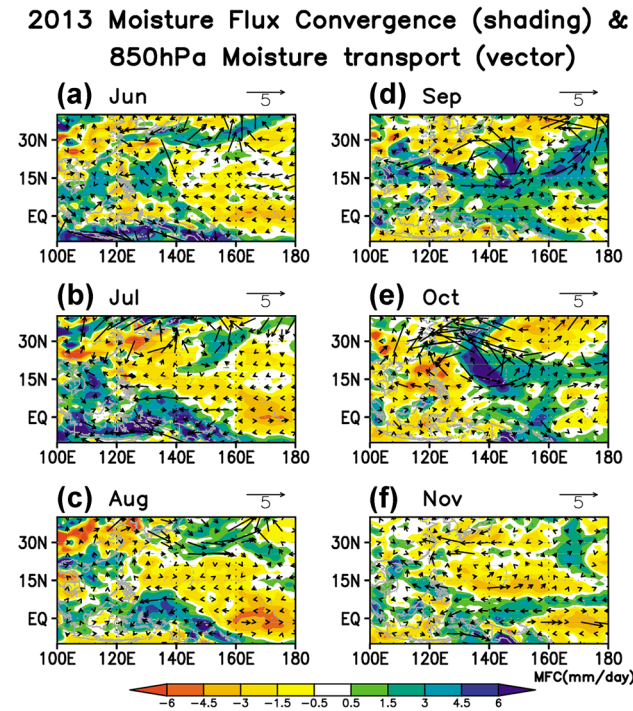
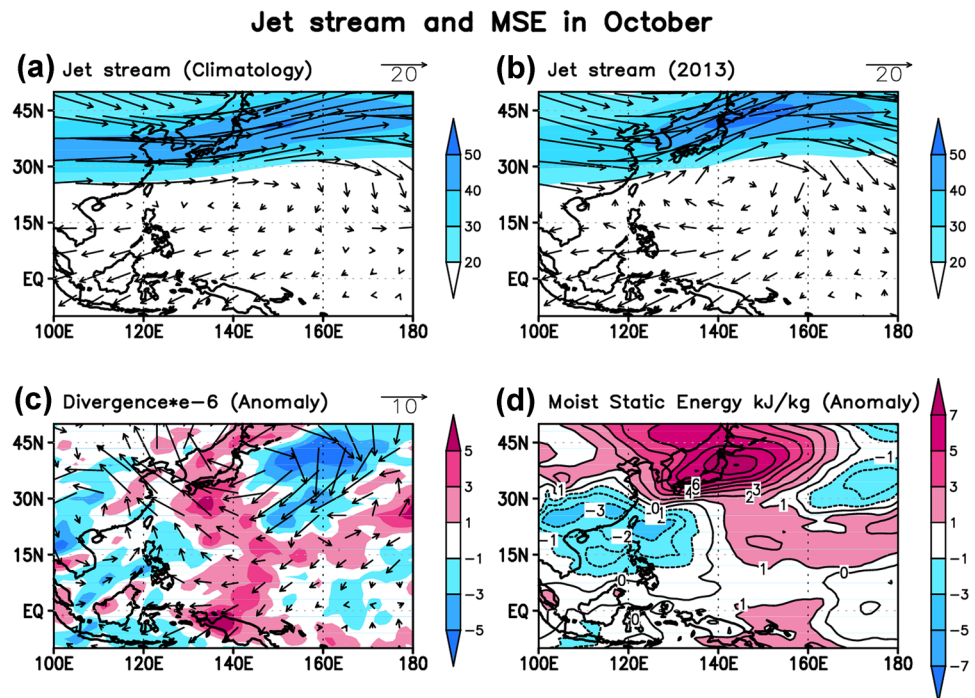


Fig. 9 Spatial distributions of 2013 monthly moisture flux convergence (MFC) (mm day^{-1} , shading) vertically integrated from 1000- to 100-hPa and 850-hPa moisture transport (10^3 ms^{-1} , vector) anomalies in (a–f) June–November

Fig. 10 Spatial distributions of (a) climatological and (b) 2013 200-hPa wind (vector, ms^{-1}) and wind speed (shading, ms^{-1}), (c) 2013 anomalous 200-hPa divergence (shading, 10^{-6}s^{-1}) and wind (vector, ms^{-1}), and (d) 2013 anomalous moist static energy (shading, kJ kg^{-1}) vertically averaged from 1000- to 500-hPa in October



Figures 11 and 12 display eight phase-space diagrams of each mode revealing the time evolution of BSISO-associated convection and circulation from May to November 2013. BSISO1 mode was remarkably enhanced in fall (Fig. 11b) compared to that in summer (Fig. 11a). In fall, BSISO1-ph6, BSISO1-ph7, and BSISO1-ph8 were linked to the genesis of six typhoons and two tropical storms occurred in September and October. However, BSISO1 was associated with the genesis of only three tropical storms in summer. Same as BSISO1 mode, about twice as many TCs occurred regarding BSISO2 mode in fall (two tropical storms and six typhoons) than those in summer (three tropical storms and one typhoon) (Fig. 12). BSISO2-ph6 was related to summer-tropical storm genesis over the East Asia, whereas BSISO2-ph8 and BSISO2-ph1 were linked to fall-typhoon genesis over the WNP and Philippine Sea. When both BSISO1 and BSISO2 were active, four typhoons occurred in September and October including two consecutive typhoon genesis (typhoon Nari and typhoon Wipha) which revealed in active BSISO2-ph8.

Figure 13 shows the composites of active BSISO1 of OLR and low-level wind anomalies with BSISO-associated genesis location of TCs. BSISO1-ph2 and BSISO1-ph5 were linked to summer-tropical storm occurred with cyclonic circulation and enhanced convection over the East Asia and South China Sea, respectively. BSISO1-ph6 showed cyclonic circulation and enhanced convection which are parallel to the latitude circle over the Philippine Sea which is characterized as the synoptic pattern in September 2013

(Figs. 3d, 9d). Indeed, all of the BSISO1-ph 6 days were selected from mid-September to mid-October. BSISO1-ph8 showed northwest–southeast oriented cyclonic circulation and enhanced convection which are characterized as the synoptic pattern in October 2013 (Figs. 3e, 9e). Indeed, most of the BSISO1-ph 8 days were selected from mid-October to late-October. It is thus conceivable that BSISO1-ph6 was linked to monsoon shear line and BSISO1-ph8 was linked to monsoon gyre. BSISO2-ph6 associated enhanced convection and cyclonic circulation over the Maritime continent and East Asia were linked to summer-tropical storm genesis (Fig. 14f), whereas BSISO2-ph1 associated enhanced convection and cyclonic circulation over the WNP were linked to typhoon genesis occurred over the eastern part of WNP (Fig. 14a). BSISO2-ph8 associated enhanced convection and cyclonic circulation were linked to two consecutive typhoon genesis (typhoon Nari and typhoon Wipha) over the Philippine Sea in the first half of October (Fig. 14h). It might help to establish the monsoon gyres in October superposing with convection and low-level wind anomalies associated with BSISO1-ph8.

5 Summary and discussion

The genesis frequency of the 2013 WNP TCs between June–August (summer) and September–November (fall) manifested an abnormal temporal asymmetry: fewer typhoons (more tropical storms) in summer and more

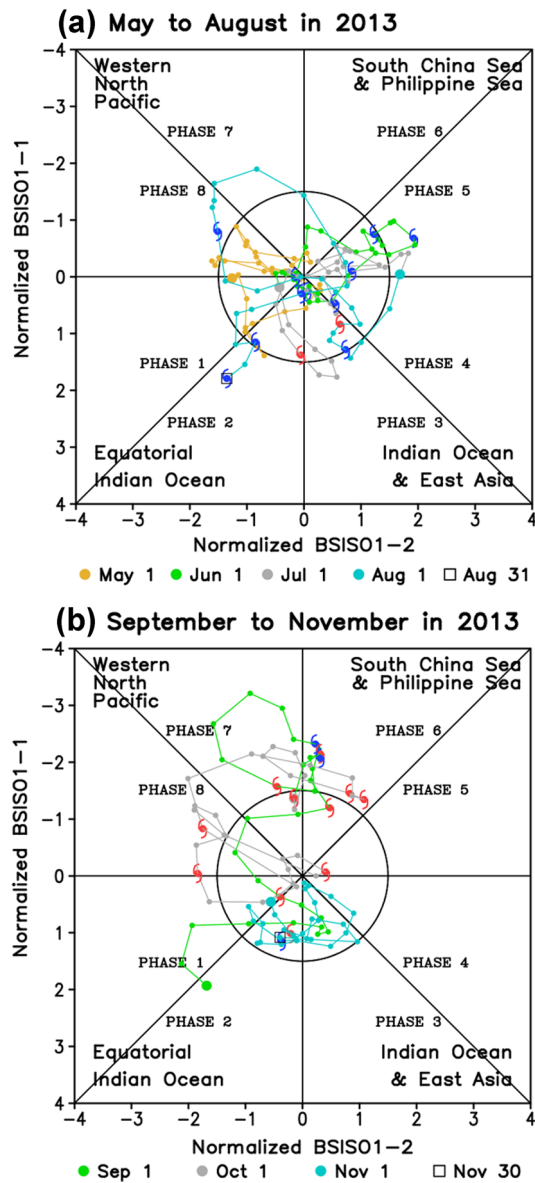


Fig. 11 Eight phases of BSISO1 defined using BSISO1-1 and BSISO1-2 indices. The phase-space curves show (a) from 1 May to 31 August and (b) 1 September to 30 November, 2013. BSISO is active when its amplitude, which is the distance from the center, exceeds 1.5 (black circle). The genesis days of typhoon and tropical storm are marked with red and blue dots, respectively

typhoons (normal tropical storms) in fall. The subseasonal asymmetry in TC genesis was investigated by using the 1979–2013 RSMC best track dataset. We examined subseasonal variations in GPI and moist thermodynamic states to demonstrate influences of large-scale environments on the subseasonal shift in TC genesis regarding the eastward-migration of convection with local SST distribution. We further investigated influence of BSISO activity on the subseasonal shift in TC genesis using the BSISO indices proposed in Lee et al. (2013).

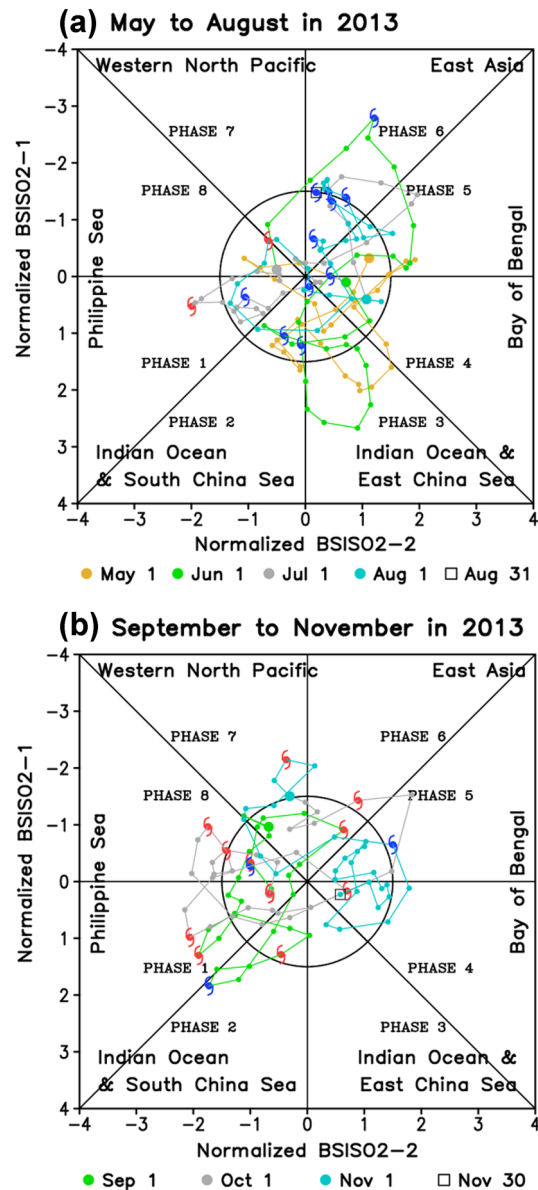
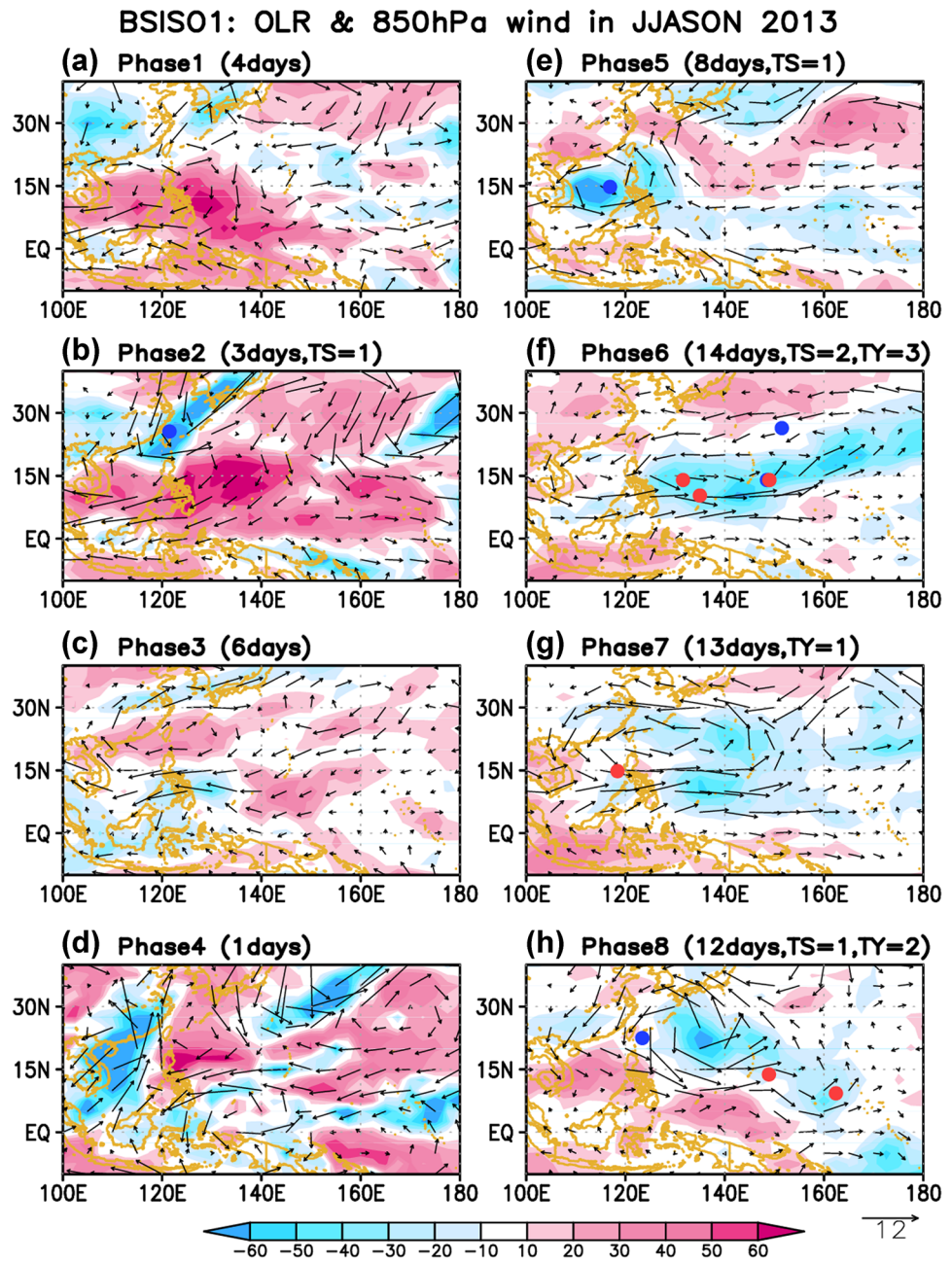


Fig. 12 Same as Fig. 11 except for BSISO2 defined using BSISO2-1 and BSISO2-2

The eastward-migration of convection from summer to fall played a crucial role in the subseasonal shift of genesis location of TCs, and consequently the 2013 temporal asymmetry in the genesis frequency between typhoon and tropical storm. The active summer-tropical storm genesis in 2013 arose from both the failure of eastward extension of monsoon confluence region, especially in August and the lack of moisture supply for TC genesis over the eastern part of WNP. The consequent westward movement of favorable location for genesis gave rise to an increase (decrease) in the number of summer-tropical storm (summer-typhoon) having less probability to reach typhoon intensity due to the relatively shorter life time. Meanwhile, the zonal wind abruptly

Fig. 13 The composites of 2013 anomalous OLR (shading, Wm^{-2}) and 850-hPa wind (vector, ms^{-1}) in (a–h) eight phases of BSISO1 (amplitude above 1.5) reconstructed based on PC1 and PC2 of BSISO. The genesis locations of typhoon and tropical storm are marked with red and blue dots, respectively

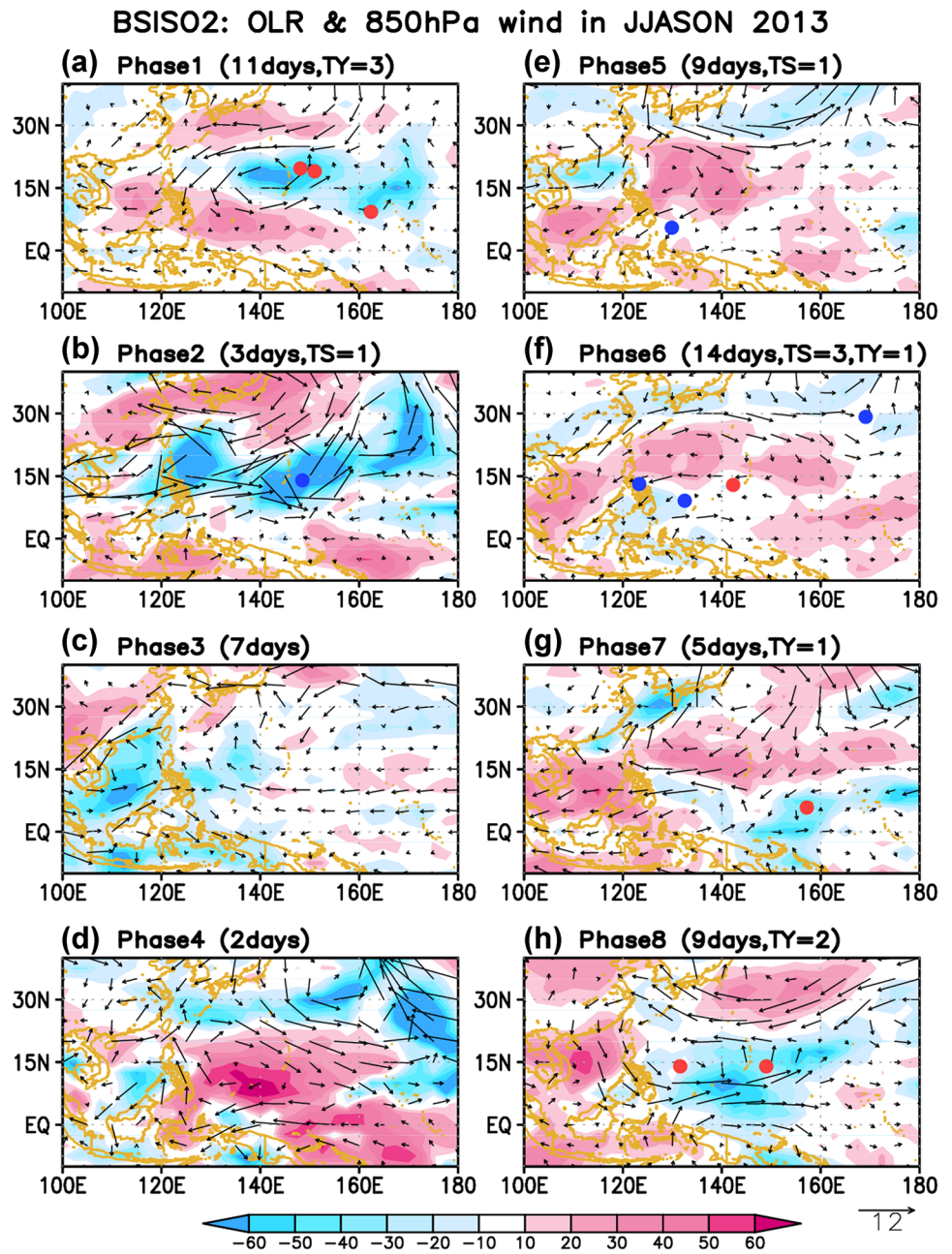


changed from easterlies to westerlies in mid-September and maintained until early November relating to both the eastward extension of monsoon shear line in September and the establishment of monsoon gyre in October. Moreover, the abundant moisture was provided by the enhanced westerlies over the main formation region with asymmetric precipitation peaked south and east of the monsoon shear line in September and east of the monsoon gyre in October. Indeed, the relative contribution of mid-level relative humidity to the positive GPI change played the major role in favorable condition for typhoon genesis in September (45.2%) and October (50.9%). The highest number of October-typhoon

associated with the monsoon gyre, which has favorable condition for genesis east of the center, leaded to the active fall-typhoon. Thus, the eastward movement of genesis location of TCs induced more probability to reach typhoon intensity due to the relatively longer life time. These spatiotemporal asymmetries in the large-scale circulation and moisture condition between summer and fall accounted for the sub-seasonal shift of genesis location of TCs, and consequently for the active summer-tropical storm genesis and the active fall-typhoon genesis in 2013.

The eastward SST gradient could play a key role in the eastward-migration of convection revealing eastward

Fig. 14 Same as Fig. 13 except for BSISO2 reconstructed based on PC3 and PC4 of BSISO



movement of local SST warming from summer to fall under the La Niña-like neutral state and very weak EIO warming in 2013. The eastward increase in convective instability (MSE) from June to October revealed the favorable thermodynamic state and high probability of typhoon genesis over the eastern part of WNP, and consequently increased the genesis frequency of typhoon in fall. It implies that the subseasonal shift in the 2013 WNP TC genesis arose from the change in local SST distribution, not the teleconnections. The north-eastward extended monsoon shear line over the warm pool in September could be superposed with lower-level cyclonic vorticity via the Gill-type response to the warm SSTA (Gill

1980) over the southeastern part of WNP and consequently evolved into the monsoon gyre in October. It is noted that the northward increase in SSTA along the 20–45°N in October decreased meridional thermal gradient, especially in the second half of October, and thus inducing the meandering subtropical jet via thermal wind balance. The meandering jet induced upper-level divergence further enhanced upward motion around the 140°E, and thus helping establishment of monsoon gyre and increasing typhoon genesis.

Regarding the BSISO activity, both BSISO1 and BSISO2 modes were remarkably enhanced in fall compared to that of summer. BSISO1-ph6, BSISO1-ph7, and BSISO1-ph8

were linked to the genesis of six typhoons and two tropical storms occurred in September and October, whereas only three tropical storms occurred associated with BSISO1 in summer. About twice as many TCs occurred associated with BSISO2 mode in fall (two tropical storms and six typhoons) than those in summer (three tropical storms and one typhoon). BSISO2-ph6 was related to summer-tropical storm genesis over the East Asia, whereas BSISO2-ph8 and BSISO2-ph1 were linked to fall-typhoon genesis over the WNP and Philippine Sea. When both BSISO1 and BSISO2 were active, four typhoons occurred in September and October including two consecutive typhoon genesis (typhoon Nari and typhoon Wipha) which revealed in active BSISO2-ph8. BSISO1-ph6 was linked to monsoon shear line and BSISO1-ph8 was linked to monsoon gyre. BSISO2-ph8 associated enhanced convection and cyclonic circulation were linked to two consecutive typhoon occurrences (typhoon Nari and typhoon Wipha) over the Philippine Sea in the first half of October (Fig. 14h). It might help to establish the monsoon gyres in October superposing with convection and low-level wind anomalies associated with BSISO1-ph8.

The variability of the number of TCs depends on both the time and region to build up enough vorticity over the MT region which thermodynamically adequate to promote convective instability as discussed in Frank and Yong (2007), and consequently cause the different variations in the genesis frequency between tropical storm and typhoon. Thus, the spatiotemporal variation in TC genesis should be understood to build water resource strategy and prevent disasters regarding impact of typhoon activity on society. Molinari and Vollaro (2017) discussed that the monsoon gyres might be regarded as the sequence of events that MJO-induced convection and vortex over the warm pool above 29 °C superposed with the climatological zonal convergence associated with the MT. The monsoon gyre could be also influenced by the mid-latitude upper-tropospheric trough penetrations (Molinari and Vollaro 2012); or it might appear a lack of physical understanding of TC genesis regarding upper-level forcing or easterly waves (Chen et al. 2008). Modeling experiment is further required in future work to determine the physical mechanism of the establishment of monsoon gyre, thus improving seasonal forecasts.

Acknowledgements This work was supported by GRL Grant of the National Research Foundation (NRF) funded by the Korean Government (MEST 2011-0021927) as well as by Global PH.D Fellowship Program through the NRF funded by the Ministry of Education (NRF-2013H1A2A1034227). We are grateful to Prof. June-Yi Lee at IBS Center for Climate Physics for providing the source code of BSISO indices (BSISO website: <http://iprc.soest.hawaii.edu/users/jylee/bsiso/>) and to the anonymous reviewers for their valuable comments and suggestions on this paper.

References

- Camargo SJ, Emanuel KA, Sobel AH (2007) Use of a genesis potential index to diagnose ENSO effects on tropical cyclone genesis. *J Clim* 20(19):4819–4834
- Camargo SJ, Wheeler MC, Sobel AH (2009) Diagnosis of the MJO modulation of tropical cyclogenesis using an empirical index. *J Atmos Sci* 66(10):3061–3074
- Cao X, Huang P, Chen G, Chen W (2012) Modulation of western North Pacific tropical cyclone genesis by intraseasonal oscillation of the ITCZ: a statistical analysis. *Adv Atmos Sci* 29(4):744–754
- Chan JCL (2008) Decadal variations of intense typhoon occurrence in the western North Pacific. *Proc R Soc A* 464:249–272
- Chan JCL (2009) Thermodynamic control on the climate of intense tropical cyclones. *Proc R Soc A* 465:3011–3021
- Chen T-C, Wang S-Y, Yen M-C, Clark AJ (2008) Are tropical cyclones less effectively formed by easterly waves in the western North Pacific than in the North Atlantic? *Mon Wea Rev* 136:4527–4540
- Choi Y, Ha K-J, Ho C-H, Chung CE (2015) Interdecadal change in typhoon genesis condition over the western North Pacific. *Clim Dyn* 45:3243–3255
- Dee DP et al (2011) The ERA-interim reanalysis: configuration and performance of the data assimilation system. *Q J R Meteorol Soc* 137:553–597
- Du Y, Yang L, Xie S-P (2011) Tropical Indian Ocean influence on Northwest Pacific tropical cyclones in summer following strong El Niño. *J Clim* 24(1):315–322
- Emanuel KA, Nolan DS (2004) Tropical cyclone activity and global climate. In: 26th conference on hurricanes and tropical meteorology. American Meteorology Society, Miami, pp 240–241 (preprints)
- Frank WM, Young GS (2007) The interannual variability of tropical cyclones. *Mon Wea Rev* 135:3587–3598
- Gill AE (1980) Some simple solutions for heat-induced tropical circulation. *Q J R Meteorol Soc* 106:447–462
- Gray WM (1968) Global view of the origin of tropical disturbances and storms. *Mon Wea Rev* 96:669–700
- Gray WM (1998) The formation of tropical cyclones. *Meteorol Atmos Phys* 67:37–69
- Ha K-J, Yoon S-J, Yun K-S, Kug J-S, Jang Y-S, Chan JCL (2012) Dependency of typhoon intensity and genesis locations on El Niño phase and SST shift over the western North Pacific. *Theor Appl Climatol* 109:383–395
- Harr PA, Wu CC (2011) Tropical cyclone characteristics and monsoon circulations. In: Chang CP (ed) The global monsoon system: research and forecast, 2nd edn. World Scientific Publishing, Singapore, pp 357–372
- Hsu P-C, Chu P-S, Murakami H, Zhao X (2014) An abrupt decrease in the late-season typhoon activity over the western North Pacific. *J Clim* 27:4296–4312
- Hsu P-C, Lee T-H, Tsou C-H et al (2017) Role of scale interactions in the abrupt change of tropical cyclone in autumn over the Western North Pacific. *Clim Dyn*. doi:[10.1007/s00382-016-3504-x](https://doi.org/10.1007/s00382-016-3504-x)
- Huang P, Chou C, Huang R (2011) Seasonal modulation of tropical intraseasonal oscillations on tropical cyclone geneses in the western North Pacific. *J Clim* 24(24):6339–6352
- Kim H-K, Seo K-H (2016) Cluster analysis of tropical cyclone tracks over the western North Pacific using a Self-Organizing Map. *J Clim* doi:[10.1175/JCLI-D-15-0380.1](https://doi.org/10.1175/JCLI-D-15-0380.1)
- Lander MA (1994) Description of a monsoon gyre and its effects on the tropical cyclones in the western north Pacific during August 1991. *Weather Forecast* 9:640–654
- Lee J-Y, Wang B, Wheeler MC et al (2013) Real-time multivariate indices for the boreal summer intraseasonal oscillation over the Asian summer monsoon region. *Clim Dyn* 40(1):493–509

- Li T, Fu B (2006) Tropical cyclogenesis associated with rossby wave energy dispersion of a preexisting typhoon. Part I: Satellite Data Analyses. *J Atmos Sci* 63:1377–1389
- Li RCY, Zhou W (2013) Modulation of western North Pacific tropical cyclone activity by the ISO. Part I: genesis and intensity. *J Clim* 26(9):2904–2918
- Li Z, Yu W, Li T, Murty VSN, Tangang F (2013) Bimodal character of cyclone climatology in the Bay of Bengal modulated by monsoon seasonal cycle. *J Clim* 26(3):1033–1046
- Liebmann B, Smith CA (1996) Description of a complete (interpolated) outgoing longwave radiation dataset. *Bull Am Meteor Soc* 77(6):1275–1277
- Lin I-I, Chan JCL (2015) Recent decrease in typhoon destructive potential and global warming implications. *Nat Commun* 6:7182
- Liu KS, Chan JCL (2013) Inactive period of western North Pacific tropical cyclone activity in 1998–2011. *J Clim* 26:2614–2630
- Maloney ED, Hartmann DL (2001) The Madden-Julian oscillation, barotropic dynamics, and North Pacific tropical cyclone formation. Part I: observations. *J Atmos Sci* 58:2545–2558
- Mao J, Wu G (2010) Intraseasonal modulation of tropical cyclogenesis in the western North Pacific: a case study. *Theor Appl Climatol* 100(3):397–411
- Molinari J, Vollaro D (2012) A subtropical cyclonic gyre associated with interactions of the MJO and the midlatitude jet. *Mon Weather Rev* 140:343–357
- Molinari J, Vollaro D (2013) What percentage of western North Pacific tropical cyclones form within the monsoon trough? *Mon Weather Rev* 141:499–505
- Molinari J, Vollaro D (2017) Monsoon gyres of the Northwest Pacific: influences of ENSO, the MJO, and the Pacific-Japan. *Pattern Clim accepted*
- Murakami H, Wang B (2010) Future change of North Atlantic tropical cyclone tracks: projection by a 20-km-mesh global atmospheric model. *J Clim* 23:2699–2721
- Oh H, Ha K-J (2015) Thermodynamic characteristics and responses to ENSO of dominant intraseasonal modes in the East Asian summer monsoon. *Clim Dyn* 44:1751–1766
- Park D-SR, Ho C-H, Kim J-H, Kim H-S (2013) Spatially inhomogeneous trends of tropical cyclone intensity over the Western North Pacific for 1977–2010. *J Clim* 26:5088–5101
- Rayner NA, Parker DE, Horton EB et al (2003) Global analyses of sea surface temperature, sea ice, and night marine air temperature since the late nineteenth century. *J Geophys Res* 108:4407
- Reynolds RW et al (2007) Daily high-resolution-blended analyses for sea surface temperature. *J Clim* 20:5473–5496
- Ritchie EA, Holland GJ (1999) Large-scale patterns associated with tropical cyclogenesis in the Western Pacific. *Mon Wea Rev* 127:2027–2043
- Roundy PE, Frank WM (2004) A climatology of waves in the equatorial region. *J Atmos Sci* 61(17):2105–2132
- Song J-J, Wang Y, Wu L (2010) Trend discrepancies among three best track data sets of western North Pacific tropical cyclones. *J Geophys Res* 115:D12128
- Wang B, Chan JCL (2002) How strong ENSO events affect tropical storm activity over the western North Pacific. *J Clim* 15:1643–1658
- Wang B, Zhang Q (2002) Pacific-East Asian teleconnection. Part II: how the Philippine Sea anomalous anticyclone is established during El Niño. *Dev J Clim* 15:3252–3265
- Wang B, Wu R, Fu X (2000) Pacific-East Asian teleconnection: how does ENSO affect East Asian climate? *J Clim* 13:1517–1536
- Webster PJ, Holland GJ, Curry JA, Chang HR (2005) Changes in tropical cyclone number, duration, and intensity in a warming environment. *Science* 309:1844–1846
- Wu L, Wen Z, Huang R, Wu R (2012) Possible linkage between the monsoon trough variability and the tropical cyclone activity over the western North Pacific. *Mon Weather Rev* 140:140–150
- Wu L, Zong H, Liang J (2013) Observational analysis of tropical cyclone formation associated with monsoon gyres. *J Atmos Sci* 70:1023–1034
- Xie S-P, Hu K, Hafner J et al (2009) Indian Ocean capacitor effect on Indo-western Pacific climate during the summer following El Niño. *J Clim* 22:730–747
- Ying M, Bai L, Zhan R (2014) Tropical cyclone activity over the western North Pacific in 2013. *Trop Cyclone Res Rev* 3(3):131–144
- Yoshida R, Ishikawa H (2013) Environmental factors contributing to tropical cyclone genesis over the Western North Pacific. *Mon Weather Rev* 141:451–467
- Yu J, Li T, Tan Z, Zhu Z (2016) Effects of tropical North Atlantic SST on tropical cyclone genesis in the western North Pacific. *Clim Dyn* 46:865–877
- Yun K-S, Seo K-H, Ha K-J (2008) Relationship between ENSO and northward propagating intraseasonal oscillation in the east Asian summer monsoon system. *J Geophys Res* 113:D14120
- Zhan R, Wang Y, Lei X (2011) Contributions of ENSO and East Indian Ocean SSTA to the interannual variability of northwest Pacific tropical cyclone frequency. *J Clim* 24:509–521
- Zong H, Wu L (2015) Re-examination of tropical cyclone formation in monsoon troughs over the western North Pacific. *Adv Atmos Sci* 32:924–934